Storm overwash of a gravel barrier: Field measurements and XBeach-G modelling

Almeida, L.P., Masselink, G., McCall, R., Russell, P.

Abstract

Gravel barriers provide a natural form of coastal protection and flood defence for many sites around the UK and worldwide. Predicting their vulnerability to different storm impact regimes that cause overtopping and overwash is crucial as these processes can lead to hazardous consequences such as inundation of the back of the barrier or breaching. This paper presents the first field measurements of storm overwash events on a gravel beach (Loe Bar, Cornwall, England). High frequency in-situ observations (2 Hz) were performed using a 2D laser-scanner and allowed a complete characterization of the overwash flows (velocity and depth) and morphological response along a cross-shore section of the barrier. These novel measurements are used to validate the numerical model XBeach-G, to forecast overwash discharge. Several simulations were performed with XBeach-G to investigate the thresholds for the different storm impact regimes, given a variety of water levels and wave heights. Wave period and wave spectral shape are found to significantly affect these thresholds. While short period waves dissipate most of their energy by breaking before reaching the swash zone and produce short runup excursions, long period waves due to their low steepness arrive at the swash zone unbroken with enhanced heights (due to shoaling) thus promoting large runup excursions. When the offshore wave spectrum has a bimodal shape, wave transformation in shallow water causes the long period peak to dominate the swash giving large runup excursions. Long period waves or strongly bimodal waves result in enhanced runup thereby reducing the thresholds for barrier overtopping or overwashing.

1. Introduction

Gravel barriers are widespread on many high-latitude, wave-dominated coasts around the world such as in the UK, Ireland, USA, Russia and New Zealand. Their shape and long-term evolution are mainly controlled by three hydrodynamic regimes: (1) swash, when runup is confined to the foreshore, resulting in berm formation and/or beach erosion, e.g., Buscombe and Masselink, (2006); (2) overtopping, when runup exceeds the crest, resulting in crest build-up and/or lowering, e.g., Matias et al., (2012); and (3) overwash, when runup exceeds the crest and promotes major modifications over the entire barrier, resulting in barrier transgression via rollover, e.g., Carter and Orford, (1993). Predicting long-term evolution of a gravel barrier therefore requires in-depth understanding of the conditions under which each of these regimes occurs. Most research on gravel barriers has focused on hydrodynamic conditions within the swash regime, mostly during mild (e.g., Austin and Masselink, 2006; Masselink et al., 2010), but more recently also under energetic wave conditions (e.g., Poate et al., 2013; Almeida et al., 2015). There is a paucity of measurements under overtopping or overwash conditions and, most of the times the observations are mostly based on pre and post-storm barrier topography (e.g., Orford et al., 2003). Bradbury (2000) has attempted to established a empirical model (Barrier Inertia Model - BIM) which relates the probability of overwash on gravel barriers to the near breaking wave steepness and the dimensionless barrier inertia parameter (ridge height x barrier area scaled against near-breaking wave height). Obhrai et al. (2008) extended the range of validity of the BIM to lower and higher steepness waves. Although this model is used in many locations in UK, the data from which was derived is site specific (Hurst Spit in the south of England). In addition to this BIM does not deal with the velocity of overwash flows and shear stress capacity at the bed (sediment size) which are key aspects regarding the wave runup on coarse-grained beaches. Is therefore possible that this model may not be valid for other gravel barriers of the coast of the UK.

55 Field observations during overtopping or overwash conditions are extremely challenge for

56 instrumentation and safety surveying operations. To overcome this limitation, research effort

57 has been devoted to the investigation of gravel barrier dynamics in controlled laboratory

58 environments (e.g., Obhrai et al., 2008 or Williams et al., 2011). These experiments have

59 provided insights into the influence of infiltration and exfiltration processes for sediment

60 transport within the swash zone (Masselink and Turner, 2012), the role of antecedent

61 conditions (overtopping and crest build up) in reducing overwash likelihood (Matias et al.,

62 2012), and the definition of thresholds for morphological changes under varying wave

63 conditions and water levels (Matias et al., 2012).

64 These laboratory datasets have also contributed to the development of the predictive skills of

65 the processed-based numerical model Xbeach (Roelvink, et al., 2009), initially developed for

66 sandy beaches, but recently adapted for gravel beaches (XBeach-G; McCall et al., 2014 and

67 2015). This model accounts for a large number of hydrodynamic processes (e.g., wave

68 transformation, groundwater interactions, runup), together with sediment transport and

69 morphological evolution, on a wave-by-wave time scale. It allows the forecast of the

70 morphological evolution of a gravel barrier under the full rangeof hydrodynamic regimes

71 (swash, overtopping and overwash), and represents a important improvement over existing

72 predictive tools (McCall et al, 2013).

73 Recent developments in field instrumentation, particularly in remote sensing techniques, have

74 demonstrated the potential to overcome traditional limitations of field experiments on gravel

75 barriers during extreme storm conditions. More specifically, the use of 2D laser-scanners to

76 measure nearshore processes enables the acquisition of high-frequency and high-resolution

77 measurements of the hydrodynamics (e.g., water level and runup) and morphological

78 evolution under extreme storm conditions (Almeida et al., 2013, 2014 and 2015).

79 This study presents new field measurements of the hydrodynamics and morphological

80 response of a fine gravel barrier (Loe Bar, Cornwall, England) under extreme impact regimes

81 (overwash) using a 2D laser scanner. These field measurements (hydrodynamics) are

82 compared with the predictions of XBeach-G, and the validated model is used to explore

83 which hydrodynamic conditions that define the thresholds for different storm impact regimes

84 (e.g., swash, overtopping and overwash) on a fine gravel barrier.

85 ## 2. Methods

86 ### 2.1.Study site and field deployment

87 The field experiment was conducted on 1 February 2014 at Loe Bar in the southwest of

88 England (Figure 1) with the aim of measuring overwash dynamics (hydrodynamics and

89 morphological response) on a gravel beach during extreme storm conditions.
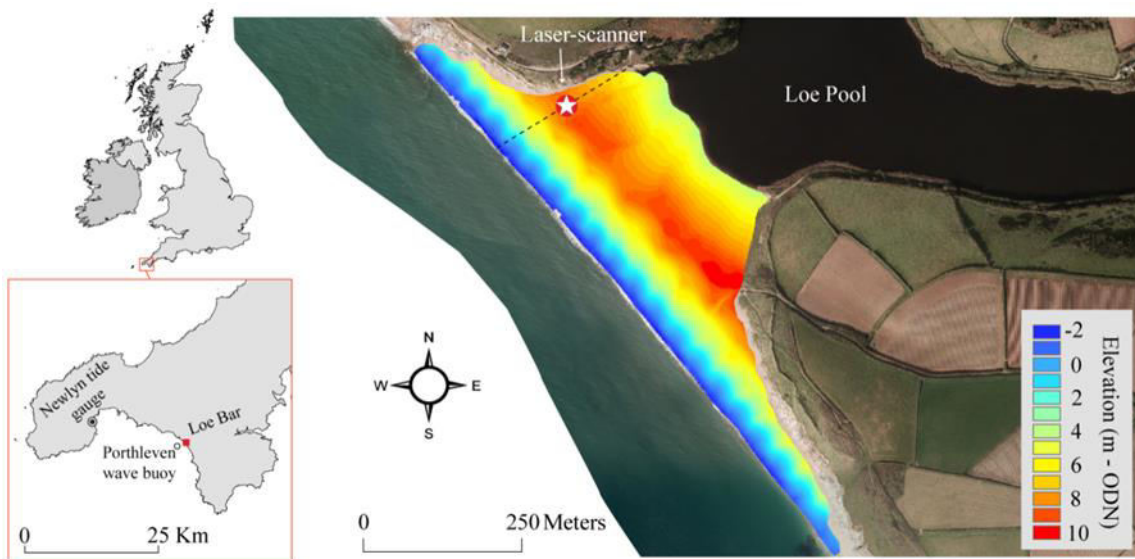
90

91 **Figure 1.**Location of the Loe Bar study site, the Porthleven wave buoy and the Newlyn tide gauge (inset maps).
92 Aerial photograph of Loe Bar with the overlap of the digital terrain model from a Lidar survey (survey
93 performed by the Channel of Coastal Observatory in 2013) with the laser-scanner position and scan profile
94 indicated.

95

96   Loe Bar is a 1 km long fine gravel (D_{50} = 2–4 mm) beach. The central section of the beach is

97   backed by Loe Pool and extends 430 m between the adjacent headlands, with an average

98   width of 250 m, a seaward gradient of 0.1, backslope gradient of 0.02 and average crest

99   elevation of 8.7 m ODN (Ordnance Datum Newlyn). The barrier is orientated 230º (SW) and

100 is exposed to energetic Atlantic swell and wind-waves with an annual average significant

101 wave height (H_s) of 1.2 m, an average peak period (T_p) of 10 s and a direction (θ_{wave}) of 235º

102 (wave statistics derived from Porthleven wave buoy measurements, October 2011 to

103 December 2014; data freely available from http://www.channelcoast.org). The tidal regime is

104 macrotidal with MHWS (mean high water spring) and MLWS (mean low water spring) at 2.5

105 m and -2.2 m ODN respectively (Ordnance Datum Newlyn; 0 m ODN ~ 0.2 m below the

106 mean sea level in UK).

107 A 2D laser-scanner (SICK - LD-OEM3100) was deployed on the top of an aluminium tower

108 (5.2 m high), fixed to a scaffold frame inserted into the beach near the barrier crest and

109 stabilized by guy ropes (Figure 2).
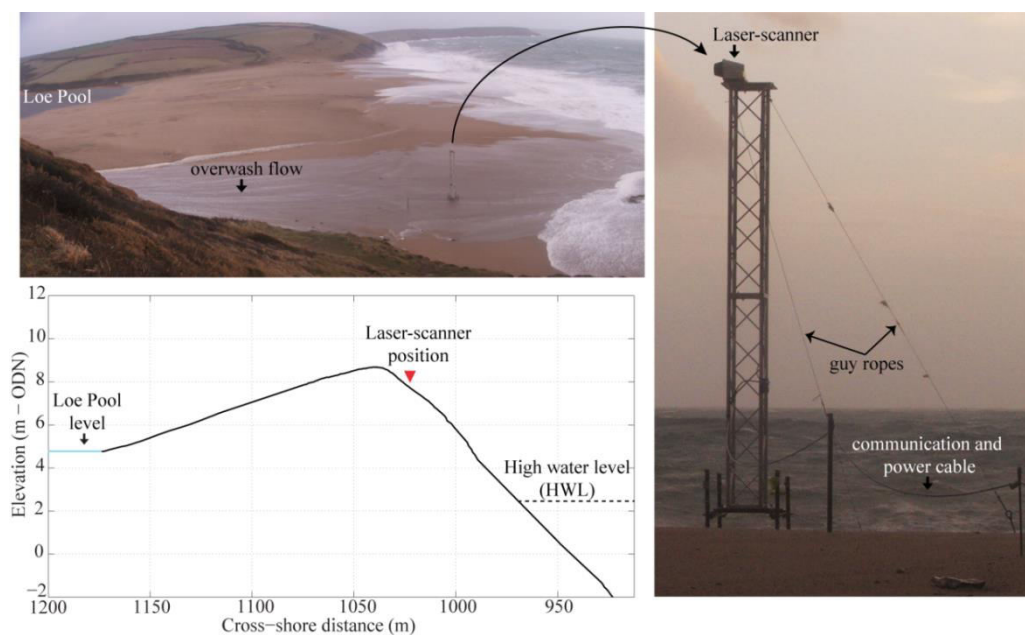
110
111 **Figure 2.** Field photographs showing the laser-scanner setup (right panel) and the deployment of the scanner on
112 the crest of Loe Bar during overwash conditions (top left panel), and detailed cross-shore profile of the barrier
113 indicating position of the laser scanner and sea and lagoon water levels (bottom left panel).

114 Offshore wave conditions were measured by the Porthleven directional wave buoy located in

115 approximately 15 m water depth at low tide (Figure 1). Due to lack of local tide

116 measurements, tide predictions for Porthleven harbour (2 km northwest of the study site)

117 were corrected by adding the meteorological tide (surge) measured at the Newlyn tide gauge.

2.2. 2D Laser-scanner and working principle

119

120 The LD-OEM3100 (manufactured by SICK) laser scanner model was selected for the present

121 work. This model is a two-dimensional mid-range (maximum range $\approx$ 100 m; SICK, 2009)

122 laser-scanner that emits pulsed laser beams (invisible infrared light; λ = 905 nm) that are

123 deflected on an internal mirror (inside the scanner head) that rotates at regular angular steps

124 and scans the surroundings (360°) in a circular manner (Figure 3). The scanner head rotates at

125 2.5 Hz with an angular resolution of 0.125° and the distance to the target is calculated from

126 the time from emission to reception of the reflection at the sensor.

127
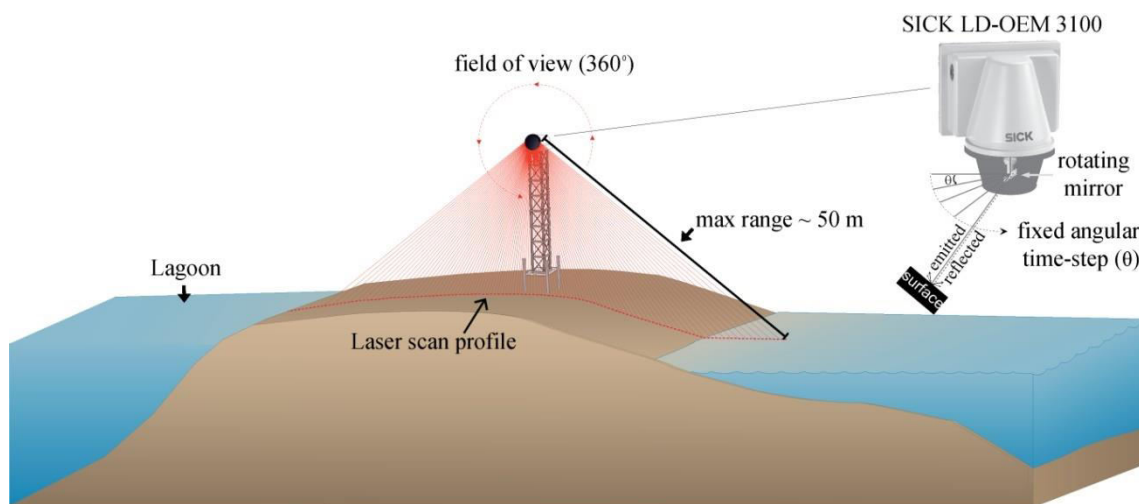
Figure 3. Sketch of the laser-scanner deployment at Loe Bar and working principles.

131   Measurements performed with the laser-scanner were processed following the method

132   presented by Almeida et al. (2015).After this initial data processing, the laser measurements

133   are separated in two distinct time series: (1) continuous beach topography; and (2) swash

134   hydrodynamics (including water elevation and runup edge). These time series form the basis

135   of the analysis of the present work.

136   An example of the type of measurements performed during this field experiment is shown in

137   Figure 4 and illustrates the ability of the laser-scanner in tracking the entire overwash process

138   (an overwash event is defined here as a single passage of water over the barrier crest).

139
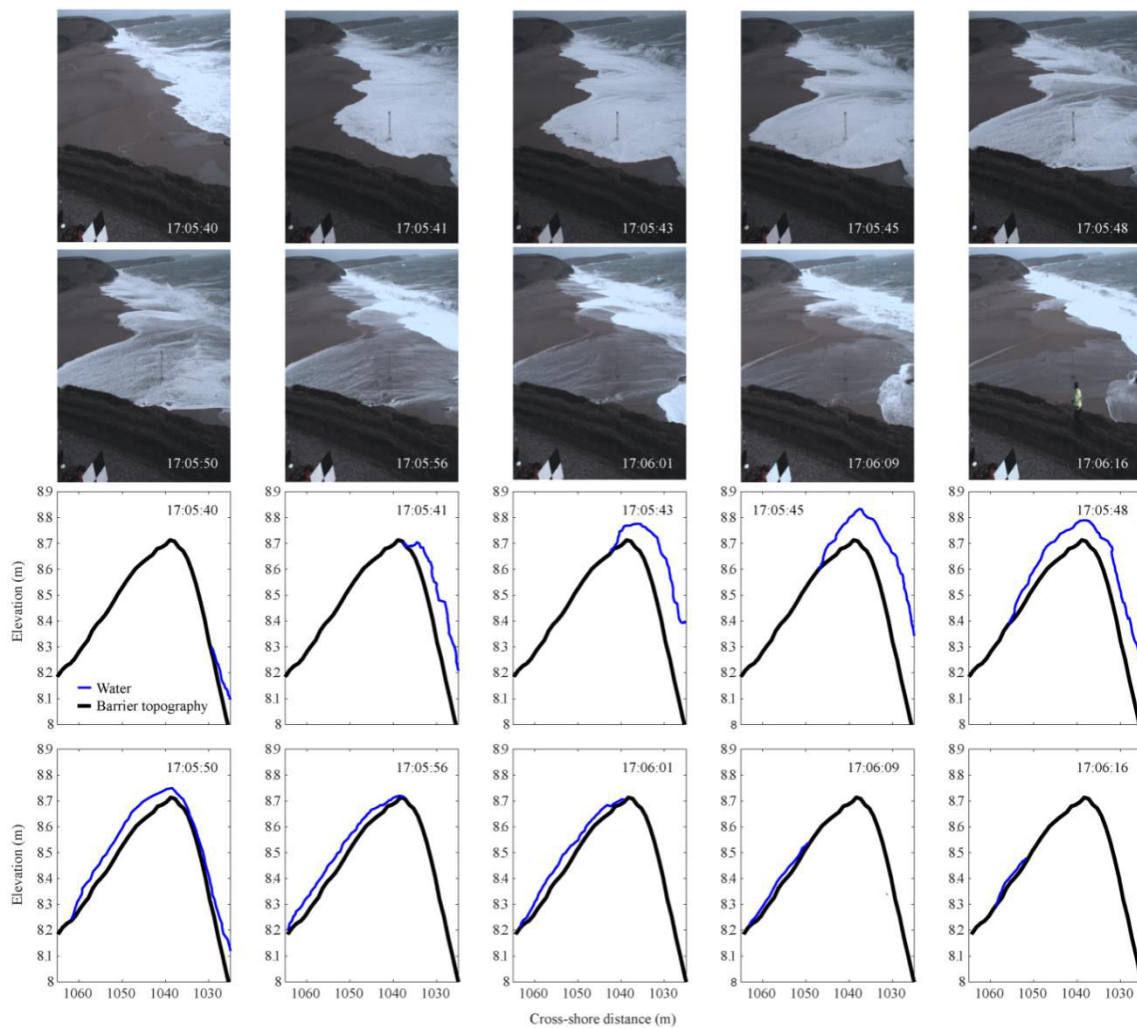
141   **Figure 4.**Sequence of video snapshots (top) and corresponding laser-scanner measurements (bottom) during an
142   overwash event over the barrier**.**

143

144 From these observations it is possible to quantify the free surface of the entire wave overwash

145 event, including the wave runup on the beach face (17:05:40-41s – Figure 4), the overtopping

146 of the crest (17:05:43s), the wave intrusion and propagation into the back of the barrier until

147 reaching the Loe lagoon (17:05:45-56s), and the infiltration on the overwash body into the

148 gravel bed on the back of the barrier (17:06:01-16s). As the water body infiltrates into the bed

149 or returns to the sea (backwash), the surface of the barrier becomes exposed, allowing the

150 laser-scanner to quantify any morphological changes (e.g., 17:06:16s).

151 **2.3. XBeach-G model**

152 To explore the impact of the full range of hydrodynamic regimes under different freeboard

153 levels on a gravel barrier, the process-based numerical model XBeach-G (McCall et al., 2014;

154 Masselink et al., 2014; McCall et al., 2015) was first validated using the field data and then

155 implemented to investigate different forcing scenarios. This model is an extension of the

156 existing Xbeach open-source storm morphodynamic model (Roelvink et al., 2009),

157 specifically adapted for gravel beaches. In contrast to Xbeach, XBeach-G uses a one-layer,

158 depth-averaged, non-hydrostatic scheme, similar to the SWASH model (Zijlema et al., 2011),

159 that allows the solution of wave-by-wave flow and surface elevation variations due to short

160 waves in the nearshore zone. This aspect is particularly important on pure gravel beaches

161 where swash motion is mainly at incident frequencies (Buscombe and Masselink, 2006). The

162 model accounts for upper swash infiltration losses and exfiltration effects on the lower swash

163 using a newly developed groundwater model coupled to Xbeach (McCall et al., 2012). Due to

164 relatively large hydraulic conductivity of coarse sediments, infiltration\exfiltration can

165 become significantly important process (e.g., Masselink and Li, 2001). The most important

166 equations implemented in XBeach-G to solve the nearshore hydro- and morphodynamics are

167 described in McCall et al. (2014)and McCall et al. (2015).

168 XBeach-G hydrodynamics (McCall et al., 2014) and morphodynamics (McCall et al., 2015)

169 have been extensively validated using laboratory (Williams et al., 2011) and field datasets

170 (Poate et al., 2013), with results showing that the model has very good skills in predicting

171 both aspects.

3. Results

3.1. Field measurements: waves, tides and laser-scanner

174 During the field experiment, storm waves from the southwest (~240°) with significant (H_s)

175 and maximum (H_{max}) wave heights of 4 m and 8 m, respectively, were recorded at offshore

176 depths (Porthleven wave buoy), with peak periods (T_p) ranging from 10 to 15 seconds (Figure

177 5). Despite the small storm surge level observed at Newlyn tide gauge (~ 0.15 m) the peak of

178 the storm coincided with the peak of a spring high tide (2.45 m), thus providing optimal

179 conditions for the occurrence of overwash events.

180 Interestingly during this storm event the offshore wave buoy recorded waves with a bimodal

181 spectrum shape (Figure 5), indicating that this event was a result of two distinct swell events,

182 one with shorter wave periods (T ~ 10 s) and another with longer wave period (T ~ 16 s –).
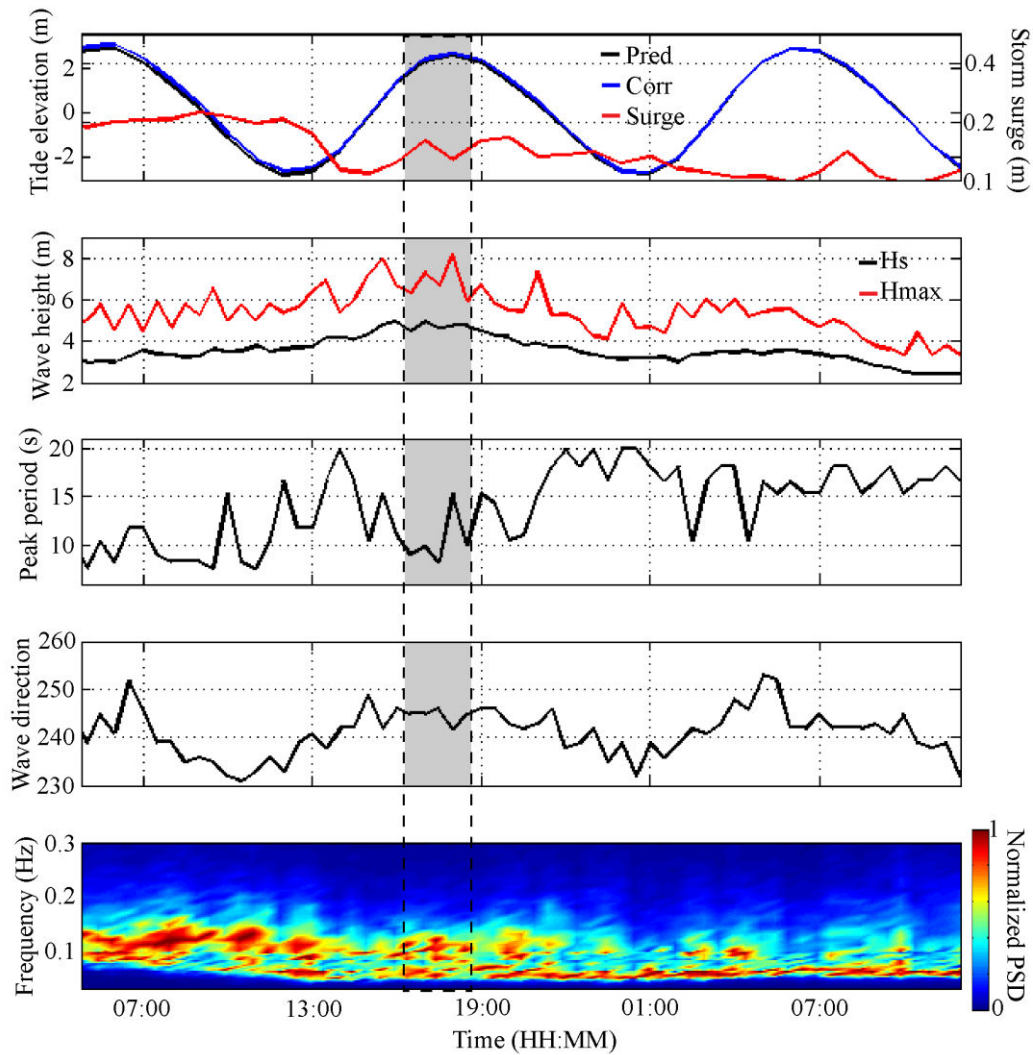
Figure 5. Corrected tide level (blue) and surge measurements (red) for Porthleven harbour - correction was performed by adding the surge computed at Newlyn gauge to the predicted tide for Porthleven harbour (top panel); offshore wave conditions, including significant and maximum wave height (second panel), peak period (third), wave direction (fourth panel) and normalised power density spectra of sea surface elevation (bottom panel), measured at Porthleven offshore wave buoy; shaded area corresponds to the period of time when laser measurements were performed.

The measurements performed with the laser-scanner lasted approximately 2 hours and 30 minutes and covered the most energetic period of the storm, during which numerous overtopping and overwash events were observed (Figure 6). Measurements include: vertical and horizontal runup excursions (R_z and R_x respectively) and morphological response.

196
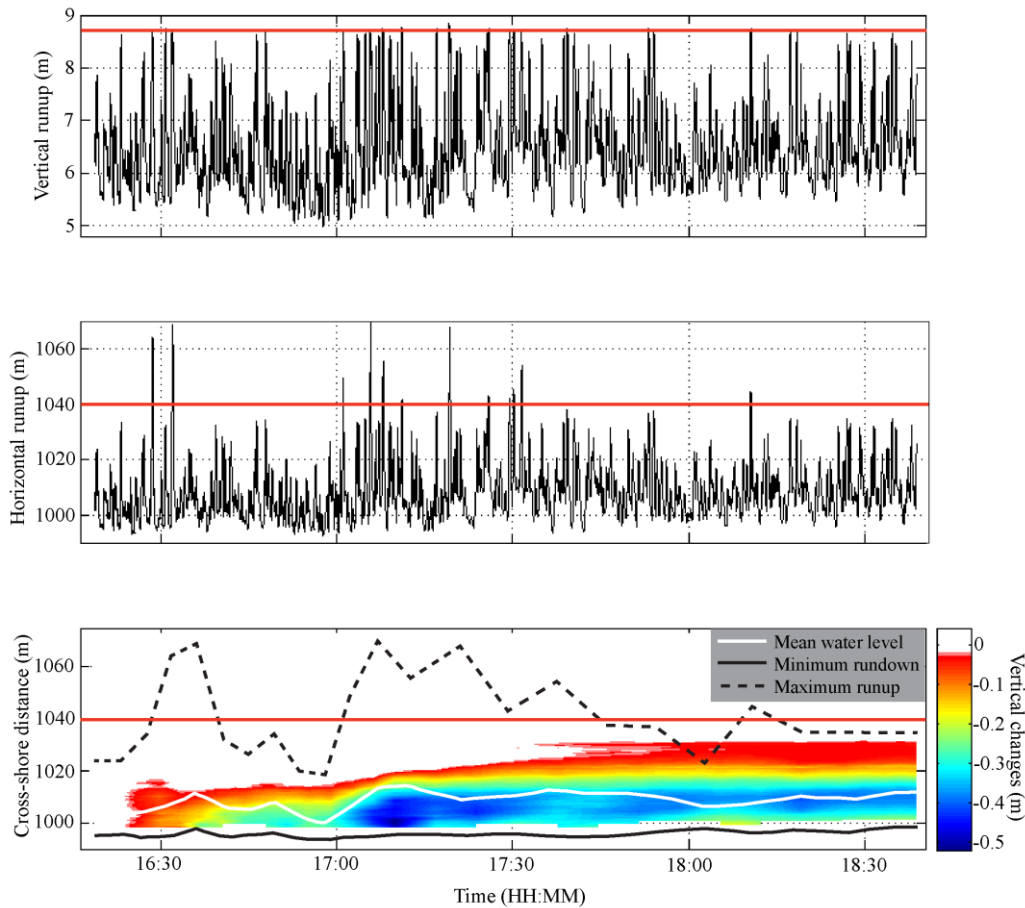
Figure 6. Vertical (top panel) and horizontal (second panel) runup excursions and morphology cumulative
changes (bottom panel) measured by the laser-scanner. Vertical datum is ODN and horizontal coordinates are in
local coordinate system (origin is located offshore at 18 m depth). Red line indicates the location of the crest of
the barrier.

Time series of vertical runup show that a large number of waves reached close to the crest of

the barrier (> 8 m ODN), although only a small percentage of these did actually overtop or

overwash the barrier, as the time series of horizontal runup illustrate (Figure 6).

The cumulative morphological changes observed by the laser-scanner during this storm event

show that the only significant modification of the barrier occurred on the seaward side of the

barrier, with the erosion of the mid swash zone (between x= 1000 and 1020 m - Figure 6).

The patch of erosion starts at approximately 16:30 when the first overwash events occurred,

and with the rising of the tide this patch moves onshore. The peak of erosion (beach erosion

210 by about 0.5 m) occurs between 17:00 and 17:30, when a group of waves overwash the

211 barrier and also when a large number of runup events reach close to the barrier crest. Since no

212 sediment accumulation was observed at the crest or back of the barrier it is likely that the

213 eroded sediment was deposited seaward from the swash (not measured by the laser-scanner).

214 One of the most important overwash parameters in determining the potential of flooding and

215 damage on the barrier is overwash discharge. Typically this parameter is measured in the

216 field by a combination of traditional *in-situ* instruments, such as electromagnetic current-

217 meters and pressure transducers (e.g., Leatherman, 1976), although recent laboratory

218 experiments suggest that these types of measurements can be estimated by semi-remote

219 sensing methods, such as ultrasonic bed-level sensors (e.g., Matias et al., 2014). In the

220 present experiment the overwash discharge was estimated by computing the product of the

221 overwash depth (h_c), measured at the crest of the barrier, and overwash leading edge velocity

222 (u_{edge}):

223

$$q_c = h_c.u_{edge} \qquad (eq.\,8)$$

224

225 Note that this method assumes that the velocity of the leading edge is representative of the

226 velocity at the barrier crest, which might not be the case when important infiltration or

227 acceleration processes (e.g. due to changes in the backslope of the barrier) affect the

228 overwash flow velocity at the leading edge. At Loe Bar it's assumed that infiltration

229 processes and the gentle back slope will not produce such modifications on the overwash

230 flow. This method has been successfully applied by other authors on gravel (Matias et al.,

231 2014) and sandy barriers (Matias et al., *in press*).

232 For each overwash event the water depth recorded by the laser-scanner at the crest of the

233 barrier (Figure 7)and velocity along the barrier was used to compute a time-series of

234 overwash discharge. An example of this type of measurement is presented in Figure 7, where

235 it is possible to observe the intrusion of one overwash event over the crest of the barrier with

236 a duration of approximately 12 seconds, maximum water depth of 0.12 m and maximum

237 velocity of 3.8 m/s, producing a mean and maximum overwash discharge of 200 L/s/m and

238 333 L/s/m respectively.

239
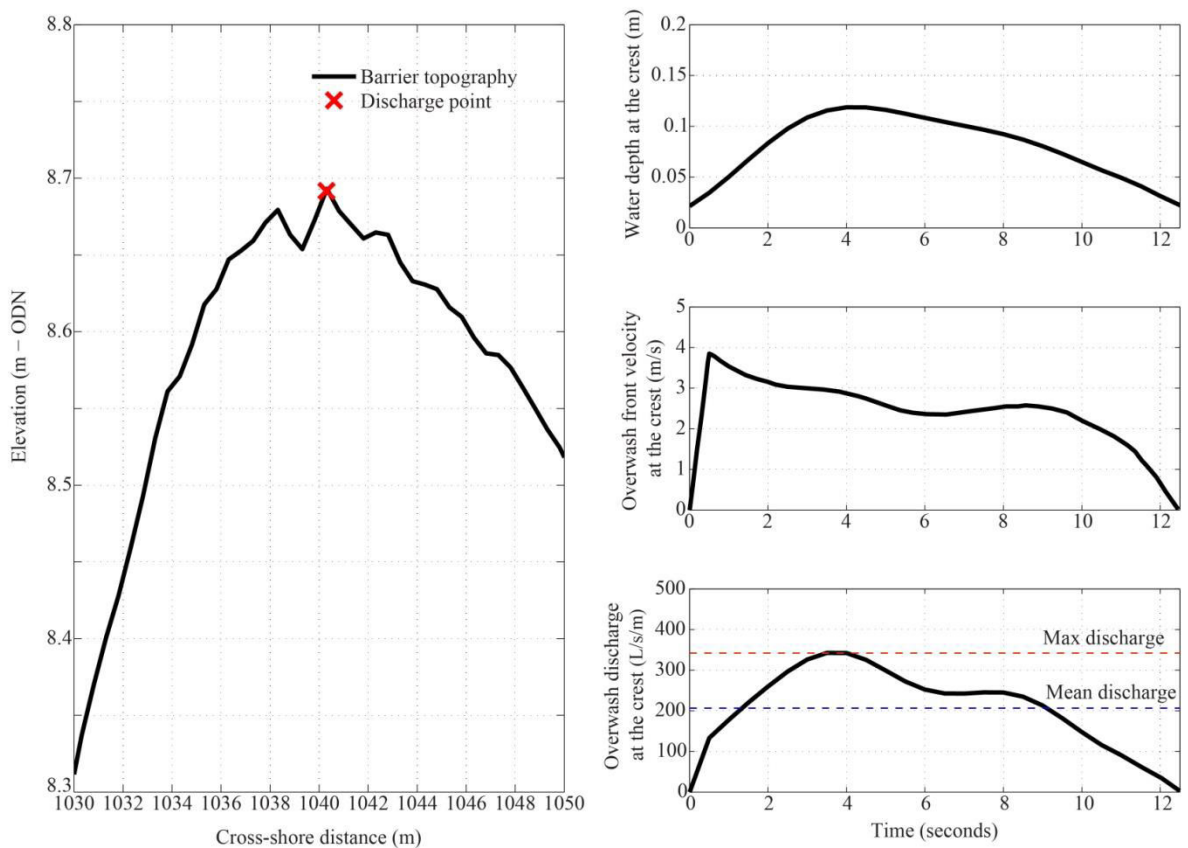
240

241 **Figure 7.**Cross-shore barrier profile with location of the point (red cross) where overwash discharge was
242 computed (left panel) and example time series of water elevation (top right panel), overwash front velocity
243 (middle right panel) and estimated overwash discharge (bottom right) for a single overwash event measured by
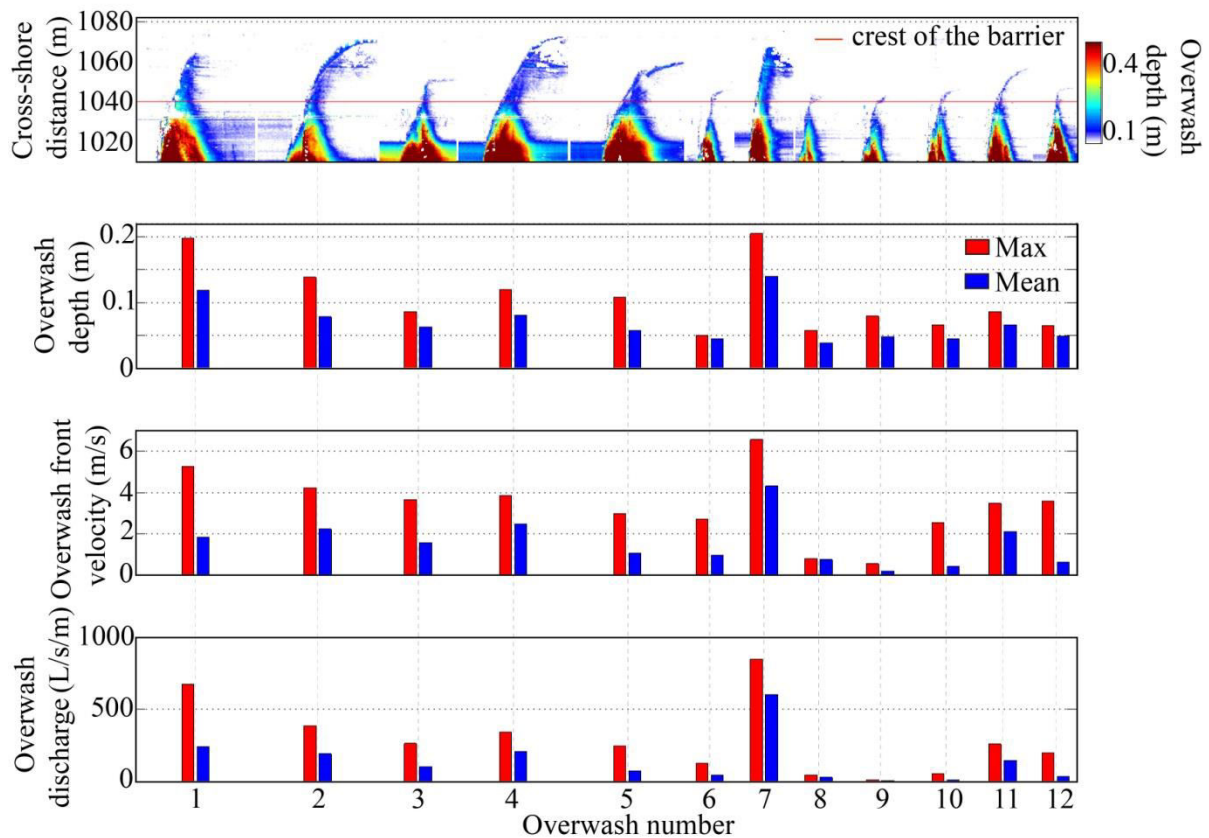244 the laser-scanner.

245

246 The same procedure was applied to compute mean and maximum overwash discharge for all

247 the overwash events measured by the laser-scanner (Figure 8). Results show that a variety of

overwash events were measured during the present field experiment, with several events overtopping the crest of the barrier but with limited horizontal intrusion across the back of the barrier (e.g., numbers 3, 6, 8, 9, 10, 11 and 12 – Figure 8), while another group had larger horizontal intrusion, reaching the Loe lagoon (overwash numbers 1, 2, 4 and 7).

Average overwash depths measured at the crest of the barrier ranged from 0.04 to 0.14 m, with maximum depths reaching 0.21 m, and average flow velocities varied from 0.05 to 4 m/s with maximum records reaching 6.3 m/s. These values are within the range of observations presented by Matias et al., (2014) as the result of a large laboratory experiment, although field measurements of these parameters have not been hitherto reported.

Figure 8. Characteristics of the overwash events measured by the laser-scanner: time series of overwash depth for each event (top panel); average and maximum overwash depth (second panel); average and maximum overwash front velocity (third panel); and average and maximum overwash discharge (bottom panel).

3.2. XBeach-G validation

The field measurements were used to validate XBeach-G by comparing measured and modelled overwash discharge, extreme runup and the frequency of overwash events.

The model bed level was set to the bed measured along the laser-scanner profile, with the sub-tidal section (measured by a previous bathymetric survey) of the profile extended to -18 m (ODN) depth (Figure 9). The cross-shore resolution of the model grid was set to vary gradually in the cross-shore direction to correctly capture wave breaking and runup in the model, with an approximately resolution of ~ 2–3 m at the offshore boundary and 0.1 m near the waterline. The grain size properties and hydraulic conductivity of the beach used in the present simulations werederived from McCall et al., 2014 (Table 1).

| D_{50} (mm)	D_{90} (mm)	K (mm s^{-1})
2	3	3

Table 1. Sediment properties used in the simulations, with grain size distributions (D_{50} and D_{90}) and hydraulic conductivity (K).

For each simulation, the model was forced with measured wave spectra retrieved from the Porthleven wave buoy, and tide predictions for Porthleven harbour, corrected for the surge levels measured at Newlyn tide gauge. Note that XBeach-G uses the input wave spectrum to generate a random time series of incident waves and bound low-frequency second order waves at the model boundary, thus comparisons with observations on an event scale are impossible.

To test the effect of considering groundwater interactions and morphological evolution, four different model setups were prepared. For Setup 1, the groundwater module was turned on and the bed was fixed during the entire duration (using the initial profile measured in the field). For Setup 2, the groundwater module was on and the morphology was continuously updated using the measured morphological changes along the laser-scan profile(rather than

287　computed sediment transport rate gradients - Figure 9), using the same approach

288　implemented by McCall et al. (2014). For Setup 3, the groundwater was turned off and the

289　profile bed was not updated. For Setup 4, groundwater was turned off and morphology was

290　updated as in Setup 2.

291
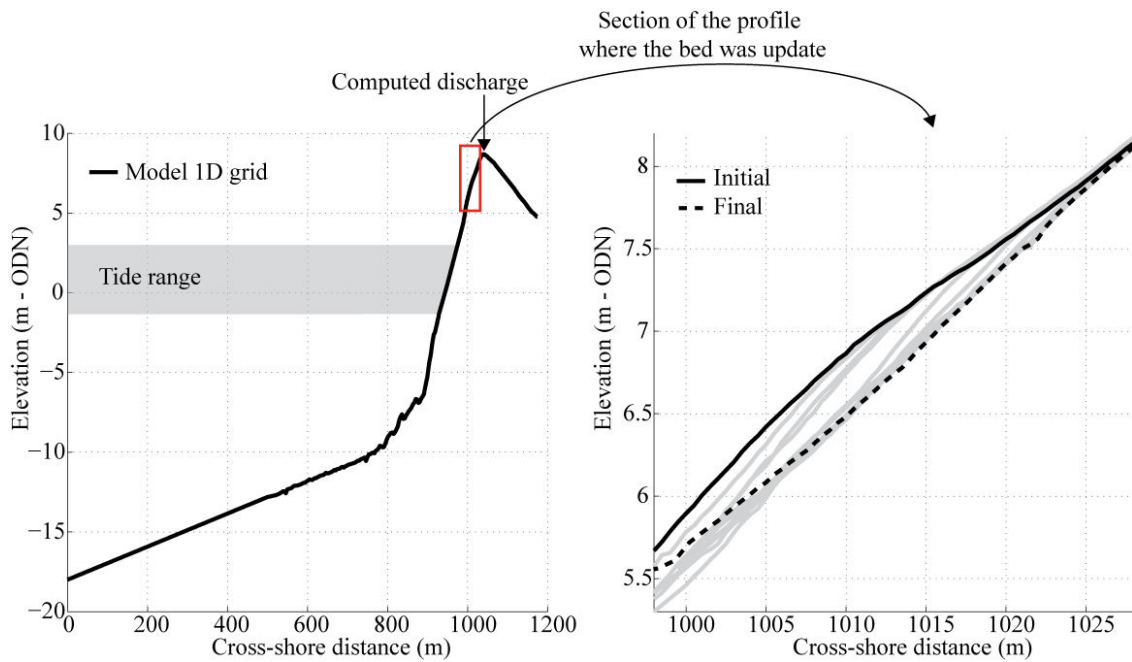
293　**Figure 9.** Cross-shore profile used for the model validation (left panel) measure before the storm event, and
294　example of the bed evolution for Setups 2 and 4 (right panel - gray lines represent the 10 minutes profile updates
295　for setup 2 and 4).

296
297　An example of the model outputs is shown in Figure 10. These results show that runup time

298　series (vertical and horizontal) present values within the range of laser measurements. It is

299　possible to verify that the average backwash limit is lower than what was observed by the

300　laser-scanner, although it is impossible to compare this aspect with the measurements, since,

301　as explained above, the laser was not able to reach the lower swash zone during this

302　experiment. Overwash discharge predictions (Figure 10) also show values within the range of

303　observations, providing a preliminary overall visual assessment of model skill.

304   In order to quantitatively compare model predictions and field observations, the following

305   parameters were computed: 1) 2% exceedance vertical runup ($R_{2\%}$), 2) number of overwash

306   events, 3) average and maximum overwash discharge, and 4) the total overwash volume

307   (computed as the integral of the discharge over the duration of each overwash event). The

308   results are presented in Table 2 and show that, in general, XBeach-G was able to reproduce

309   results close to the field observations.

310   The extreme runup predicted by XBeach-G slightly underestimates the field observations

311   (4.6% less when groundwater was on and less than 3% when groundwater was off – Table 2)

312   and therefore this was also reflected on the number of overwash events predicted by the

313   model and the total volume of water that overwashed the barrier. The only exception was the

314   model simulations using groundwater off and no bed update (Setup 3), which predicted

315   exactly the same number of overwash events as were measured in the field (Table 2).
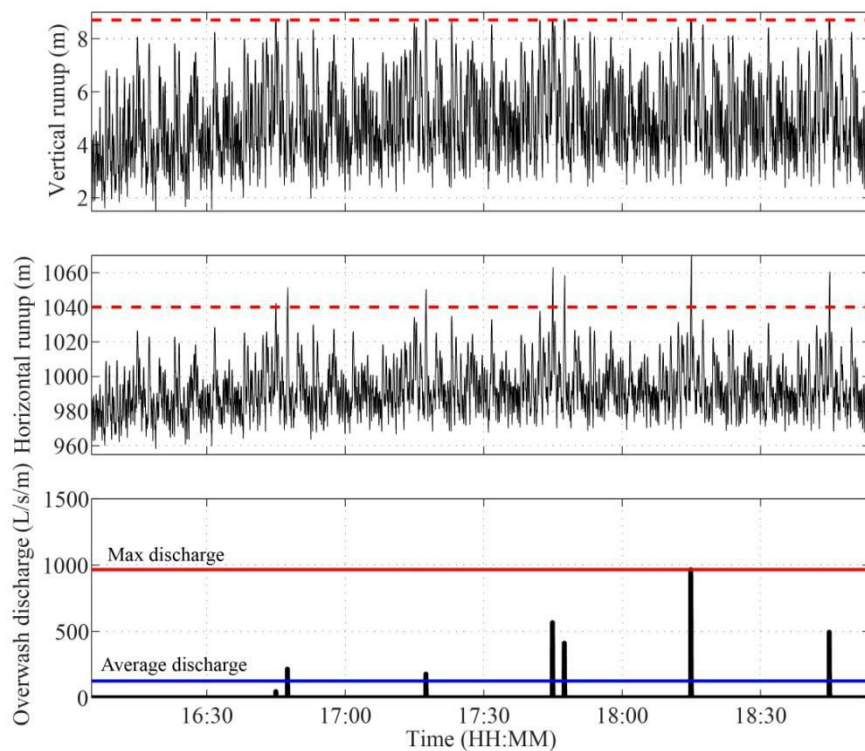
Figure 10 Example of XBeach-G output for the simulations with Setup 1, showing the time series of vertical
(top panel) and horizontal (middle panel) runup and the overwash discharge (bottom panel) computed for the
storm conditions observed during the present experiment. Red dashed line indicates the position and elevation of
the barrier crest.

321 The results show that average and maximum overwash discharge was better predicted when

322 the model was using groundwater on and slightly overestimated the maximum overwash

323 discharge when the groundwater was set off (Table 2).

324

	Measured	Setup 1	Setup 2	Setup 3	Setup 4
Morphology	-	fixed	update	fixed	update
Groundwater	-	on	on	off	off
$R_{2\%}$ (m)	6.5	6.2	6.2	6.4	6.3
Overwash events	12	7	7	12	10
Average discharge (L/s/m)**	140	120	100	110	70
Maximum discharge (L/s/m)**	840	960	880	1260	1210
Volume (L)	17550	9071	8485	17203	16121

325 **Table 2.**XBeach-G model validation results for the four different types of model setup.** Discharge is the
326 average for the period of time that measurements were performed.

327

3.3.UsingXBeach-G to investigate overtopping and overwashing discharge under variable wave height and water levels

330

331 Wave runup can exceed the barrier crest under storm and non-storm conditions, when the

332 combination of the water levels and wave conditions allows this (Morton et al., 2000). To

333 investigate and quantify the conditions under which the Loe Bar barrier overwashed, 64

334 XBeach-G simulations were performed, using combinations of eight significant wave heights

335 (H_s 1–8 m) and eight water levels (1–8), and a fixed peak wave period (T_p = 10 s) and mean

336 wave period (T_m = 8.4 s; representing the average wave period calculated from 4 years of

337 measurements at Porthleven wave buoy). Each model was setup using the measured pre-

338 storm profile (Figure 9), and the forcing waves were characterized by the standard unimodal

339 Jonswap spectrum (gamma = 3.3). Each model was run for 5400 s (1 h and 30 min) with

340 stationary water level, with the initial 1800 s used to spinup the model and the remaining

341 3600 s for analysis.

342 Figure 11 shows the results of the simulations by means of a contour map of overwash

343 discharge under variable water levels and wave heights. To contextualize these discharge

344 values in terms of potential damage to the barrier (e.g. damage to the crest or back of the

345 barrier), three main hydrodynamic regimes that occur at Loe Bar barrier under storm or non-

346 storm conditions are identified. Swash regime is representative of cases when runup is

347 confined to the foreshore, when no overtopping is observed (white area on the map - Figure

348 11), while overtopping and overwash regimes describe conditions when the wave runup

349 exceeds the crest of the barrier.
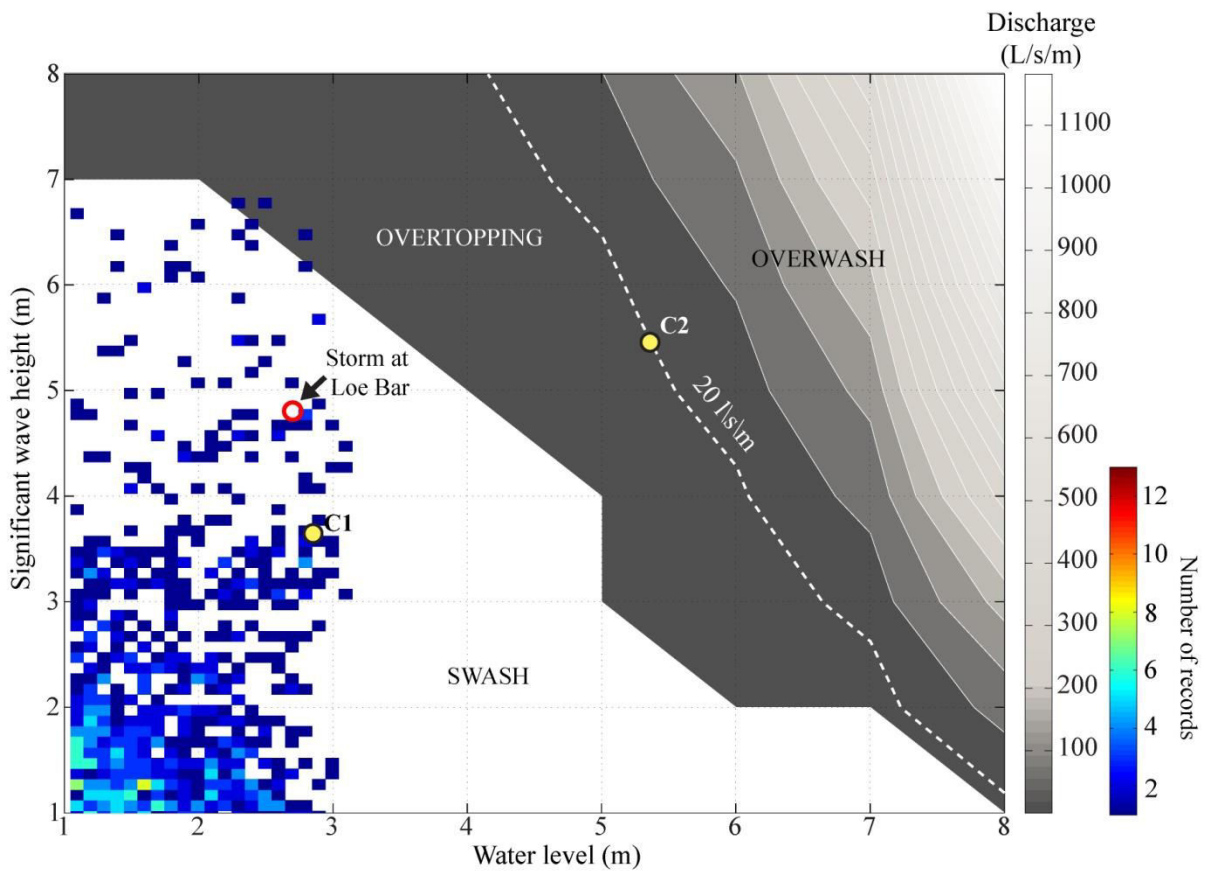
350

351 **Figure 11.** Contour map of the average wave overtopping and overwash discharge under different significant
352 wave height and water level conditions, overlain by a bivariate histogram of measured H_s and water level for
353 waves with $T_p > 10$ s (wave data source: Porthleven wave buoy; tide source: Newlyn tide gauge). The yellow
354 filled circles represent the mid-regime forcing conditions for which the effect of changing wave period, spectral
355 shape and groundwater interactions will be explored later in this work.

356

357 To identify the boundary between overtopping and overwash regime, the approach used by

358 McCall et al., (2013) was followed. It defines the threshold for overwash discharge based on

359 engineering guidelines for the stability of rip-rap structures under overwash conditions.

360   According to these guidelines (Simm, 1991; Frizell et al., 1998), an average overwash

361   discharge above 20 L/s/m is expected to cause severe damage to the crest and back of the

362   barrier; therefore, that value was used here to define the threshold for an overwash regime.

363   By overlapping the joint distribution of waves and tides (based on four years of wave and

364   tide measurements, for $T_p > 10$ s) on the discharge map (Figure 11), it is clear that only a very

365   small number of actual observations lie within the overtopping domain, and none inside the

366   overwash regime. A preliminary interpretation of this result is that Loe Bar has an extremely

367   low vulnerability to overtopping and overwash events. This assumption is supported by

368   recent studies performed at this site (e.g., Poate *et al.*, 2013 or Almeida *et al.*, 2015), which

369   observed a lack of overtopping even under energetic wave conditions.

370   Interestingly, on the current discharge map, the present storm measurements fall within the

371   swash regime (red dot − Figure 11), when, according to field measurements and model

372   validation (Table 2), this result should be within an overwash regime. An important

373   difference between the model setup during the validation section and the regime analysis was

374   the fact that, in the validation section, the bimodality of the offshore wave spectrum was

375   taken in account, whereas, on the discharge map, the simulations were performed using a

376   unimodal spectrum shape.

377   Previous authors have shown bimodality of offshore wave spectra to be an important factor

378   when considering the prediction of wave runup on gravel beaches (Polidoro et al., 2013) and

379   potentially the overtopping discharge (Masselink et al., 2014).

380   To investigate why the present storm conditions do not fall within theoverwash regime in

381   Figure 11, two new model simulations were performed using a bimodal Jonswap wave

382   spectrum with similar shape to the measured wave spectrum (measured at Porthleven wave

383   buoy) and another model using a unimodal Jonswap wave spectrum with equivalent energy

384   (identical H_s and T_m - Figure 12).

385   The results of these two model simulations show that overwash discharge at the crest occurs

386   when the model was forced with a bimodal wave spectrum, but no discharge when a

387   unimodal wave spectrum was used (Figure 12). This result confirms that the presence of a

388   bimodal wave spectrum can enhance the occurrence of overwash. The fact that the present

389   storm did not fall within the overtopping regime was merely due to the present regime map

390   being produced with unimodal wave spectrum shape.
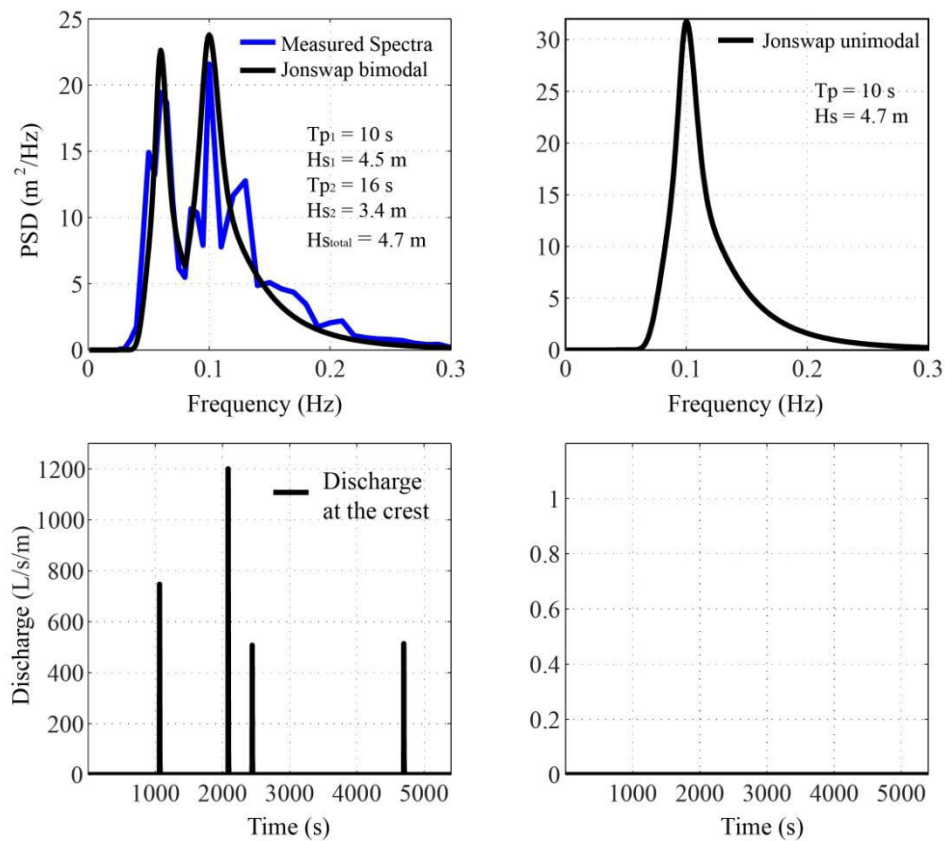
391

392   **Figure 12.** Results of the overtopping discharge (lower panels) computed using a bimodal (top left panel) and
393   unimodal Jonswap spectra (top right panel) with the same T_m = 10 s and H_s = 4.5, using gamma = 2.

394

395   The wave spectrum was computed for each time series of water elevations predicted for each

396   cross-shore position of the grid, and is presented in Figure 13. The results show that, for the

397   bimodal wave forcing, the lower frequency energy increases towards the shore (from x = 600

398   to 900 m), whereas the shorter frequency energy dissipates. The swash zone becomes

399   dominated by the longer period waves, producing a wider swash zone, and there is

400   development of infragravity waves. When the model was forced with the unimodal wave

401   spectrum, the peak period waves were dissipated significantly before reaching the swash zone

402   (between x = 0 and 600 m), and swash zone width is slightly narrower than that which

403   developed under bimodal wave spectrum. No apparent development of energy on the

404   infragravity band was found under unimodal wave spectrum conditions and no overwash

405   occurred. These results put also in evidence the importance of the wave steepness regarding

406   the wave runup processes.While on the bimodal spectrum the low steepness (long period)

407   wavesdominate the swash and promote large runup excursions that overtop the barrier, on the

408   unimodal casesteeper waves (short period waves) are unable to overtop the barrier.
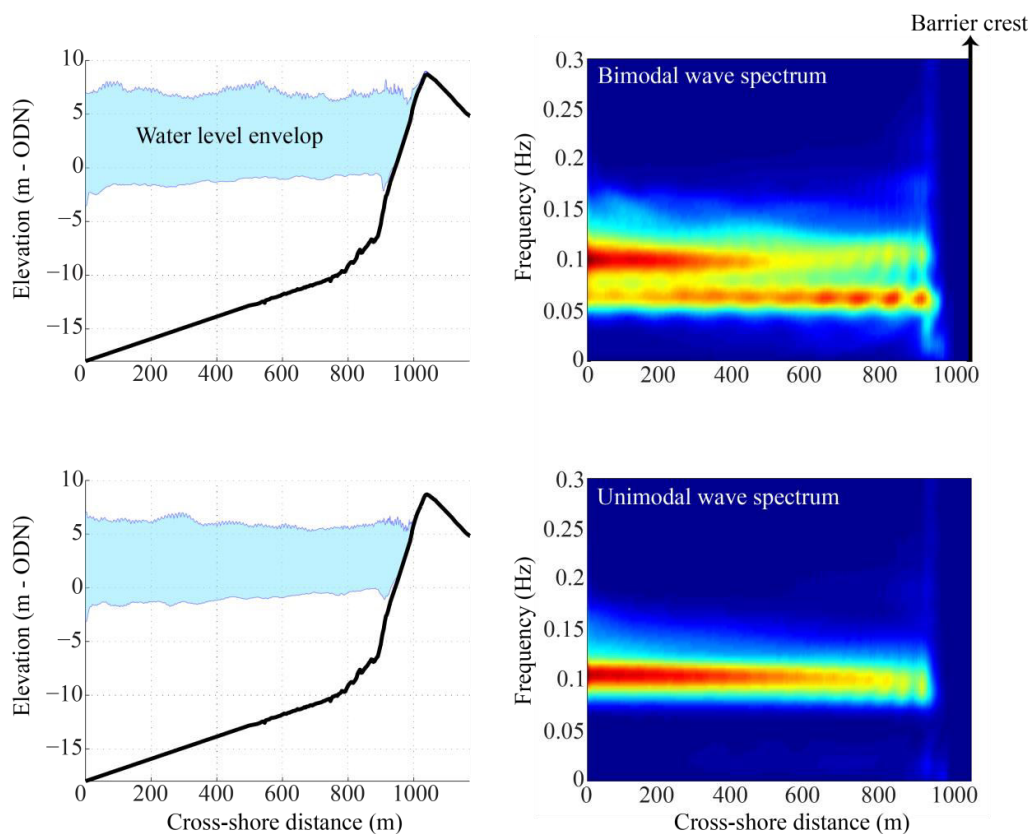

409

410   **Figure 13.**Wave spectrum computed for each time series of water elevations predicted for each cross-shore
411   position of the grid from the model outputs presented in Figure 14.

3.4. XBeach-G: The effect of wave period, spectral shape and groundwater on the definition of storm impact regimes

To quantify the effect of wave period, spectral shape and groundwater on the impact regimes identified in Figure 11, a new set of XBeach-G model runs was formulated. Two categories of simulations were defined (C1 and C2), and for each category a representative value of water level and H_s was used as a constant during all the simulations (see filled yellow circles in Figure 11). To enable a fair comparison between the different spectral shapes, the mean period T_m ($T_m = m_0/m_1$), where m_1 and m_0 represent the first and zero moment of the wave spectrum, respectively) was kept constant, independently of whether a bimodal or unimodal spectrum was employed.

To test the role of wave period, a total of 20 XBeach-G models were set up (10 per category) for 10 classes of T_m (from 5–12 s) using a standard unimodal wave spectrum (Figure 14). The 20 simulations were carried out both with and without the groundwater module turned on. Finally, an additional of 60 simulations was set-up to investigate the role of spectral shapes on swash and overwash dynamics. In addition to the unimodal wave spectrum, two bimodal Jonswap spectra were designed by adding a long period swell ($T_{p(swell)}$ = 15 s) to the unimodal spectrum (Figure 14).
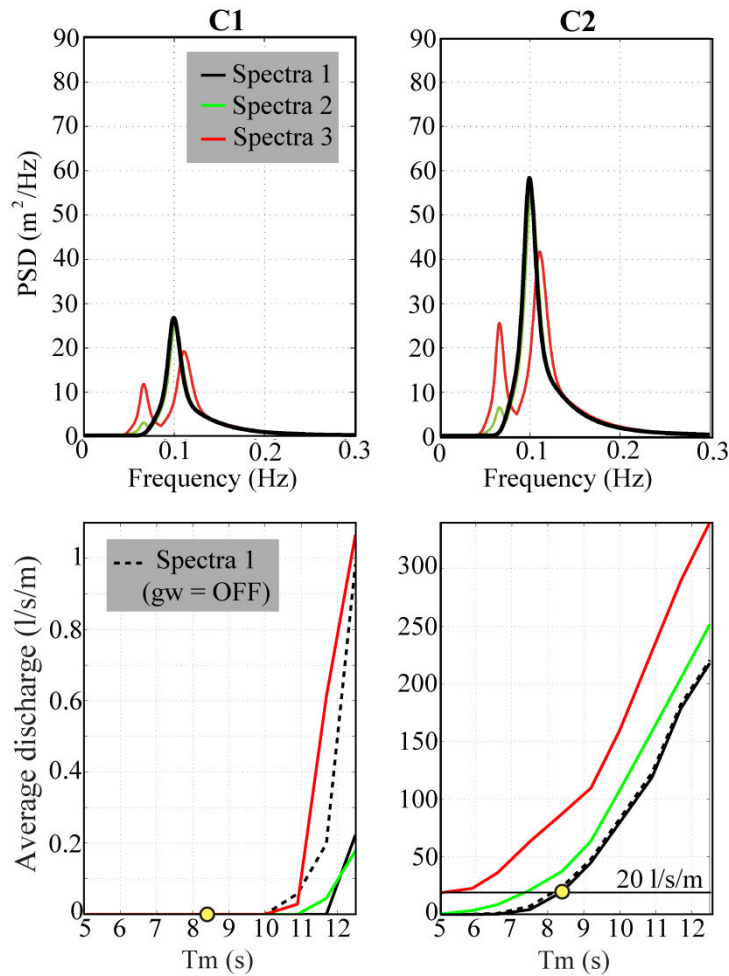
Figure 14. Shape of the three different wave spectrum tested for each category of simulations(top panels); Results of discharge under variable T_m values for the two different categories, testing different parameters: typical Jonswap spectra with groundwater ON (black line); with groundwater OFF (dashed grey line); and testing different wave spectral shapes (red, blue and green lines). The yellow dots represent the category valuescomputed for Figure 11.

Care was taken to ensure that the addition of the long period swell peak was balanced by a reduction in the wave height and period of the short period wind peak to ensure that the significant wave height and the mean wave period remained the same. The groundwater module for these additional 90 simulations was turned on and off.

Each simulation was run for 5400 s (1h 30m), with the first 30 minutes to spinup the model (these data were removed from the analysis), and for each simulation the average discharge was computed at the crest of the barrier.

444 The average overwash discharge for the three different hydrodynamic regimes for variable

445 wave periods (with and without groundwater) and spectral shapes are presented in Figure 14.

446 The results show that wave period and spectral shape can produce significant modifications

447 on the predicted average discharges, and change the boundaries of the impact regimes

448 presented in Figure 11. Increasing both wave period and energy in the swell peak enhances

449 the likelihood of overtopping and overwashing, and increases overwash discharge.

450 Groundwater interactions only seem to have a significant effect on the swash regime

451 (category C1), when large T_m values are tested, but under overtopping or overwash regimes

452 (C2 simulations) the inclusion of groundwater interaction does not produce a significant

453 difference in modelled discharge (Figure 11).

454 4. Discussion

455 In the first section of this work, a new and unique dataset of field measurements of storm

456 runup and overwash events on a gravel barrier (Loe Bar) is presented. This dataset was

457 subsequently used to validate the XBeach-G model predictions of hydrodynamics. The

458 validated model was then used to explore the hydrodynamic conditions under which this

459 gravel barrier is exposed to different impact regimes (swash, overtopping or overwash). This

460 model analysis also included the investigation of the model's sensitivity to wave period,

461 spectral shape and groundwater dynamics.

462 4.1. Measuring wave overtopping on a gravel barrier with a laser-scanner

463 During this experiment, 12 overwash events were recorded by a new remote sensing

464 technique, 2D laser-scanner. The laser-scanner measurements provided coverage of an entire

465 cross-section of the barrier, enabling the detection of overwash flow from the top of the beach

466 face to the back of the barrier. Due to the limited range of this laser-scanner (~ 50 m), the

467 amount of information (e.g., backwash limit, morphological change in the lower swash zone)

468   collected from the lower beach face was small, restricting further analysis from that section

469   of the barrier.

470   Despite the lack of ground-truth validation of the present laser-scanner observations, previous

471   laboratory and field experiments have shown that this instrument enable a robust detection of

472   the swash edge (e.g., Almeida et al., 2015 or Hofland et al., 2015) and swash depth (e.g.,

473   Vousdoukas et al., 2014 or Brodie et al., 2015). It is known that the laser beam penetrates the

474   water surface to some extent and is then refracted according to Snell's law, causing a possible

475   source of errors (Streicher, 2013). The penetration depth is controlled by the turbidity and the

476   water surface roughness (Irish et al., 2006), which are two factors characteristic of

477   overtopping and overwash flows (large content of suspended sediment and turbulent foamy

478   bores). Under this conditions strong laser returns are expected to occur just at the surface of

479   the water (Vousdoukas et al., 2014).

480   Due to the absence of field observations of overwash hydrodynamics on gravel beaches

481   worldwide, the present observations may only be compared with earlier measurements

482   performed on sandy beaches or laboratory experiments. The average overwash velocities

483   measured during the present field experiment (Figure 8) are of the same order as those

484   measured in the field on sandy barriers (Leatherman, 1977; Leatherman and Zaremba, 1987;

485   Holland et al., 1991; Bray and Carter, 1992; Matias et al., 2010), where mean velocities

486   varied between 0.5 and 3 m/s, and in laboratory tests using sandy (Srinivas et al., 1992; or

487   Donnelly, 2008) and gravelly sediments (Matias et al., 2014), where average overtopping and

488   overwash velocities ranged from 0.8 and 3.6 m/s.

489   In regard to overwash depths, earlier field observations performed on sandy barriers yielded

490   peak flow depths ranging from 0.10 m to 0.7 m (Fisher and Stauble, 1977; Matias et al.,

491   2010; or Bray and Carter 1992), leaving the present observations within the lower range of

492   values (maximum depths of approximately 0.20 m – Figure 8).

493   These comparisons provide confidence that this remote sensing technique is suitable for

494   measuring these processes on gravel barriers under challenging field conditions.

495   **4.2. The use of XBeach-G to predict overtopping and overwash on a gravel**
496   **barrier**

497   Comparison between the XBeach-G predictions and the field observations presented in this

498   work show some encouraging results, that demonstrate that XBeach-G has skills in predicting

499   the hydrodynamics of this gravel barrier under storm conditions. Despite the limited number

500   of overwash events observed during this storm, the model was capable of reproducing these

501   events (with some level of under-prediction).

502   Using the most complete model setup (Setup 2 – with bed update and groundwater on), the

503   model was able to predict extreme runup ($R_{2\%}$) with only a 5 % underestimation of the

504   observations (Table 2). Modelled averages and maximum overtopping discharge at the crest

505   were also very close to what was measured in the field. Such results are in line with recent

506   validation efforts performed with XBeach-G hydrodynamics, indicating that the model is

507   capable of reproducing wave transformation, runup and overtopping with an average error <

508   10% (McCall et al., 2012; McCall et al., 2014).

509   **4.3. Defining storm impact regimes on Loe Bar**

510   The initial approach was to quantify the overtopping and overwashing discharge under

511   different combinations of water level and wave height for a certain wave period (Figure 11).

512   With this 'map' it was then possible to define the three boundaries, based on discharge, that

513   separate the three different impact regimes. These boundaries were defined using existing

514   engineering guidelines that relate average overwash discharge at the crest of defence

515   structures (e.g., dikes) with morphological responses.

516   The resulting impact regime diagram was then compared with the joint distribution of wave

517   height and tide level for the Loe Bar location. This comparison indicated that, according to

518   the XBeach-G model, overtopping/overwashing conditions on Loe Bar are extremely

519   unlikely because this requires unrealistically high water levels (Figure 11). An detail

520   investigation on the effect of wave spectral shape allowed to identify that wave spectrum

521   bimodality can magnify the discharge predictions and modify significantly the definition of

522   the these thresholds (Figure 14).

523   This particular aspect has been previously identified along the south coast of England as an

524   important factor linked to coastal flooding hazards (Hawkes et al., 1998; Masselink et al.,

525   2014). In the present work, this particular aspect is explored by the validated XBeach-G

526   model (Figure 10). The main difference between the unimodal and bimodal spectrum across

527   the nearshore is shown to be the differential mechanism of wave dissipation that both spectra

528   present (Figure 11). While in a bimodal spectrum the short period peak (the peak period)

529   tends to dissipate the energy before arriving to the swash (due to breaking), the long period

530   peak gains due to shoaling processes (Lorenzo, et al., 2001). The result of this differential

531   dissipation of the two peaks of the spectrum causes the long-period peak to become dominant

532   in the swash zone, increasing the vertical runup excursions and swash width (Figure 11).This

533   process is very well captured by XBeach-G numerical model (McCall et al., 2014) which,

534   beyond other important parameters, includes non-hydrostatic pressure correction term that

535   allows wave-by-wave modelling of the free surface elevation, allowing the simulation of the

536   whole wave spectrum, including variable spectral shapes.

537

4.4. Predicting wave runup on gravel barriers

Predicting accurately the extreme runup on gravel or sandy barriers during extreme storms is crucial to assess the vulnerability of these environments to destructive hazards such as overwashes. On the sandy barriers across the North America the U.S. Geological Survey (USGS) perform this evaluation through the application of the storm impact scale model developed by Sallenger (2000), which implements the Stockdon et al. (2006)to predict the storm induced maximum runup excursions. The same runup equation was recently validated for gravel barriers after extensive testing of different runup equations (Matias et al., 2012).

Shortcomings in the application of Stockdon et al. (2006) on gravel barriers may arise from aspects such as the complex nearshore or foreshore features (e.g., several berms) or the effect of wave spectral shape that are not taken in consideration by this runup equation (Plant and Stockdon, 2015).

The comparison between extreme runup observations presented in this work and predictions performed with XBeach-G and Stockdon et al. (2006) runup equation show that the latter (based on peak wave period) underestimates significantly the runup elevation (Figure 15).

553
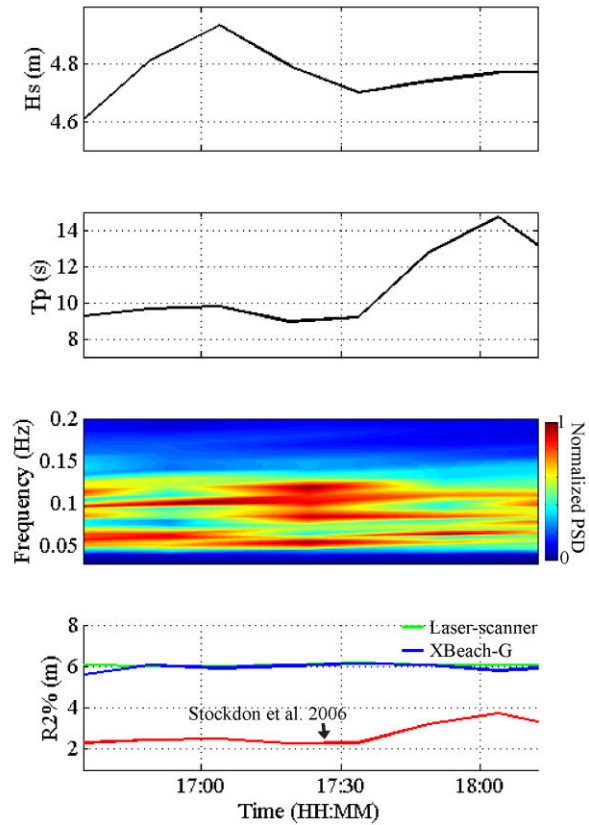
Figure 15. Comparison between vertical runup observations and predictions using Stockdon et al., (2006) runup equation and XBeach-G numerical model (bottom panel), forced with 2 hours of wave measurements (performed at Porthleven wave buoy) during the measured storm; Stockdon et al., (2006) runup equation was implemented using significant offshore wave height (top panel), peak period (second panel), while XBeach-G used the full wave spectra (third panel).

Potential reasons for such evident underestimation is the fact that Stockdon et al. (2006) equation was not validated for extreme waves ($H_s > 3$ m), and very important processes such as the wave bimodality is not taken in account on this formulation. From all these reasons the latter assume particular importance since in the present work it was demonstrated with the XBeach-G model wave spectrum shape can affect significantly the forecast of wave runup.

5. Conclusion

This work presents unique field observations of overtopping and overwash events during a storm on a gravel barrier. These measurements allowed a validation of XBeach-G for this gravel barrier, which showed great skill in predicting hydrodynamics (< 5% error) during storm events where overtopping and overwash occur.

The boundaries between the different impact regimes (swash, overtopping and overwash) were explored for a fine gravel beach, Loe Bar, using XBeach-G. Hundreds of model simulations demonstrate that these boundaries are not only the result of the combination between water level and wave height, but that wave period and spectral shape also play key roles. Wave bimodality encourages the development of higher wave runup and wider swash zones dominated by long-period water motions, enhance the likelihood of overtopping and overwash, and increase the associated discharge. While short period waves dissipate most of their energy by breaking before reaching the swash zone and produce short runup excursions, long period waves due to their low steepness arrive at the swash zone unbroken with enhanced heights (due to shoaling) thus promoting large runup excursions. When the offshore wave spectrum has a bimodal shape, wave transformation in shallow water causes the long period peak to dominate the swash giving large runup excursions.

Present modelling efforts allowed to demonstrate that on fine gravel beach like Loe Bar the groundwater have limited effect on the extreme runup and definition of the thresholds for storm impact regimes.

Acknowledgements

References

Almeida, L., Masselink, G., Russell, P., Davidson, M., Poate, T., McCall, R., Blenkinsopp, C., Turner, I., 2013.Observations of the swash zone on a gravel beach during a storm using a laser-scanner.Journal of Coastal Research, 65, 636–641.

Almeida, L.P., Masselink, G., Russell, P., Davidson, M., McCall, R., Poate, T., 2014. Swash zone morphodynamics of coarse-grained beaches during energetic wave conditions. Proceedings to International Conference on Coastal Engineering, Seoul, South Korea.

Almeida, L.P., Masselink, G., Russell, P., Davidson, M., 2015. Observations of gravel beach dynamics during high energy wave conditions using a laser scanner. Geomorphology, 228, 15-27.

Austin, M.J., Masselink, G., 2006. Swash–groundwater interaction on a steep gravel beach.Continental Shelf Research, 26, 2503–2519.

Bradbury, A., 2000. Predicting breaching of shingle barrier beaches — recent advances to aid beach management Papers and Proceedings 35th MAFF (DEFRA) Conference of River and Coastal Engineers, 05.3.1–05.3.13.

Bray, T.F., Carter, C.H., 1992. Physical processes and sedimentary record of a modern, transgressive, lacustrine barrier island. Marine Geology, 105, 155–168.

Brodie, K.L., Raubenheimer, B., Elgar, S., Slocum, R.K., McNinch, J.E., 2015. Lidar and pressure measurements of inner-surf zone waves and setup. Journal of atmospheric and ocean technology, 32, 1945-1959.

Buscombe, D., Masselink, G., 2006. Concepts in gravel beach dynamics. Earth Science Reviews, 79, 33–52.

Carter, R.W.G., Orford, J.D., 1993. The morphodynamics of coarse clastic beaches and barriers: a short- and long-term perspective. Journal of Coastal Research, 15, 158-179.

Donnelly, C., 2008. Coastal Overwash: Processes and Modelling. Lund University, Sweden (53 pp. + papers).

Fisher, J.S., Stauble, D.K., 1977. Impact of Hurricane Belle on Assateague Island washover.Geology, 5, 765–768.

Frizell, K.H., Ruff, J.F., and S. Mishra, 1998. Simplified design guidelines for riprap subjected to overtopping flow. Proceedings of the Annual Conference of the Assoc. of State Dam Safety Officials, 301–312.

Hawkes, P.J., Coates T.T., Jones, R.J., 1998. Impact of bi-model seas on beaches and control structures. Research report SR 507, HR Wallingford.

Hofland, B., Diamantidou, E., van Steeg, P., Meys, P., 2015. Wave runup and wave overtopping measurements using a laser scanner. Coastal Engineering, 106, 20-29.

Holland, K.T., Holman, R.A., Sallenger, A.H., 1991. Estimation of overwash bore velocities using video techniques. Proceedings of Coastal Sediments '91, USACE, Seattle,Washington, USA, 489–497.

Irish, J.L., Wozencraft, J.M., Cunningham, A.G., Giroud, C., 2006.Non intrusive measurement of ocean waves: lidar wave gauge. Journal of Atmospheric and Oceanic Technology, 23, 1559–1572.

Leatherman, S.P., 1976. Quantification of overwash processes. Charlottesville, Virginia: Department of Environmental Sciences, University of Virginia, PhD dissertation, 245.

Leatherman, S.P., 1977. Overwash hydraulics and sediment transport. Proceedings of Coastal Sediments '77. ASCE, Charleston, USA, 135–148.

Leatherman, S.P., Zaremba, R.E., 1987. Overwash and aeolian processes on a U.S. Northeast coast barrier. Sedimentary Geology, 52, 183–206.

Lorenzo, A., Meer, J., and Hawkes, P. (2001) Effects of Bi-Modal Waves on Overtopping: Application of UK and Dutch Prediction Methods. Proceedings to International Conference on Coastal Engineering, 2114-2127.

Matias, A., Ferreira, Ó., Vila-Concejo, A., Morris, B., Dias, J.A., 2010. Short-term morphodynamics of non-storm overwash. Marine Geology, 274, 69–84.

Matias, A., Williams, J.J., Masselink, G., Ferreira, Ó., 2012. Overwash threshold for gravel barriers. Coastal Engineering, 63, 48–61.

Matias, A., Blenkinsopp, C., Masselink, G., 2014. Detailed investigation of overwash on a gravel barrier. Marine Geology, 350, 27-38.

Matias, A., Masselink, G., Castelle, B., Blenkinsopp, C.E., Kroon, A., *in press*. Measurements of morphodynamic and hydrodynamic overwash processes in a large-scale wave flume. Coastal Engineering.

Masselink, G., Russell, P., Blenkinsopp, C.E., Turner, I.L., 2010. Swash zone sediment transport, step dynamics and morphological response on a gravel beach. Marine Geology, 274, 50–68.

Masselink, G., Turner, I.L., 2012. Large-scale laboratory investigation into the effect of varying back-barrier lagoon water levels on gravel beach morphology and swash zone sediment transport. Coastal Engineering, 63, 23–38.

Masselink, G., McCall, R., Poate, T., van Geer, P., 2014. Modelling storm response on gravel beaches using XBeach-G.Proceedings of the Institution of Civil Engineers Maritime Engineering, 1-19.

McCall, R., Masselink, G., Poate, T., Bradbury, A., Russell, P., Davidson, M., 2013.Predicting overwash on gravel barriers. Journal of Coastal Research Special Issue No. 65 Proceedings 12th International Coastal Symposium,1473–1478.

McCall, R., Masselink, G., Poate, T., Roelvink, D., Almeida, L.P., 2015.Modelling storm morphodynamics of gravel beaches during storms with XBeach-G. Coastal Engineering, 103, 52-66.

McCall, R., Masselink, G., Poate, T., Roelvink, J., Almeida, L., Davidson, M., Russell, P., 2014.Modelling storm hydrodynamics on gravel beaches with XBeach-G. Coastal Engineering, 91, 231-250.

Morton, R.A., Gonzalez, J.L., Lopez, G.I., Correa, I.D., 2000. Frequent non-storm washover of barrier islands, Pacific coast of Columbia. Journal of Coastal Research, 16, pp. 82-87.

Obhrai, C., Powell, K., Bradbury, A., 2008. A laboratory study of overtopping and breaching of shingle barrier beaches.Proc.Coast. Eng. ASCE, Hannover, Germany, 1497–1508.

Orford, J., Jennings, S.C., Pethick, J., 2003. Extreme storm effect on gravel-dominated barriers. Final Proc. of the International Conference on Coastal Sediments, St Petersburg, United States, 1-12.

Plant, N., Stockdon, H.F., 2015. How well can wave runup be predicted? Comment on Laudier et al. (2011) and Stockdon et al. (2006).Coastal Engineering, 102, 44-48.

Poate, T.,Masselink, G., Davidson, M., McCall, R., Russell, P., Turner, I., 2013. High frequency in-situ field measurements of morphological response on a fine gravel beach during energetic wave conditions. Marine Geology, 342, 1–13.

Polidoro A, Dornbusch U and Pullen T (2013) Improved maximum run-up formula for mixed beaches based on field data. In Allsop W and Burgess K (eds). Proceedings of the ICE Breakwaters Conference.

Roelvink, D., Reniers, A., van Dongeren, A., de Vries, J.T., Mccall, R., Lescinski, J., 2009. Modelling storm impact on beaches, dunes and barrier islands. Coastal Engineering, 56, 1133–1152.

Sallenger, A.H., 2000. Storm impact scale for barrier islands. Journal of Coastal Research, 16, 890–895.

Streicher, M., Hofland, B., Lindenbergh, R.C., 2013.Laser ranging for monitoring water waves in the new Deltares Delta flume. Proceedings to ISPRS Workshop Laser Scanning, Antalya, Turkey, 271-276.

Stockdon, H.F., Holman, R.A, Howd, P.A. and Sallenger Jr., A. H., 2006.Empirical parameterization of setup, swash and runup. Coastal Engineering, 53, 573–588.

SICK, 2009.LD-OEM1000 to 5100 Laser Measurement System – operating manual.SICK AG Waldkirch, Germany.

Simm J. D. (Editor), 1991. Manual on the use of rock in coastal and shoreline engineering.CIRIA special publication 83, CUR Report 154.

746 Srinivas, R., Dean, R.G., Parchure, T.M., 1992. Barrier Island Erosion and Overwash
747 Study.Volume 1.Coastal and Ocean Engineering Department, University of Florida, 92.

749 Vousdoukas, M.I., Kirupakaramoorthy, T., Oumeraci, H., 2014.The role of combined laser
750 scanning and video techniques in monitoring wave-by-wave swash zone processes. Coastal
751 Engineering, 83, 150–165.

753 Williams, J.J., Buscombe, D., Masselink, G., Turner, I.L., Swinkels, C., 2011. Barrier Dynamics
754 Experiment (BARDEX): aims, design and procedures. Coastal Engineering, 63, 3–12.

756 Zijlema, M., Stelling, G. and P. Smit. 2011. SWASH: An operational public domain code for
757 simulating wave fields and rapidly varied flows in coastal waters. Coastal Engineering, 58,
758 992–1012